



Experimental and Analytical Study of Temperature Swing Piston Coatings in a Medium-Duty Diesel Engine

Aravindh Babu, Georgios Koutsakis, Sage Kokjohn, and Michael Andrie University of Wisconsin-Madison
Engine Research Center

Citation: Babu, A., Koutsakis, G., Kokjohn, S., and Andrie, M., "Experimental and Analytical Study of Temperature Swing Piston Coatings in a Medium-Duty Diesel Engine," SAE Technical Paper 2022-01-0442, 2022, doi:10.4271/2022-01-0442.

Received: 25 Jan 2022

Revised: 25 Jan 2022

Accepted: 09 Jan 2022

Abstract

The use of Thermal Barrier Coatings (TBCs) has been shown to be a promising technology to improve internal combustion engine efficiencies by reducing heat rejection to the coolant and oil. In recent studies, temperature swing coatings that have simultaneously low volumetric heat capacity and low thermal conductivity have been shown to be particularly promising in this regard. In this study, a traditional and a newer swing coating are applied to the piston of an on-road medium-duty diesel engine to assess the benefits of their use. An analytical wall temperature model is coupled

to the 1-D engine simulation software GT-POWER and predictions of wall temperature, heat transfer and chemical heat release rate are presented. The swing coating is found to yield an ~1.2% efficiency benefit at the highest load condition studied alongside an 80°C improvement in exhaust temperature at the lowest load condition studied compared to a reference uncoated piston. Further, the traditional TBC was not found to have a significant efficiency advantage over the reference uncoated piston, highlighting the promise of the swing coating in improving the thermal efficiency of on-road diesel engines.

Keywords

Thermal Barrier Coating; TBC; Temperature Swing Coating; TSC; CDC; GT-POWER

Introduction

The utilization of Internal Combustion Engines is predicted to increase due to increasing global trade and economic growth of developing markets [1]. Many agencies and industrial groups show future transportation fuel demand is likely to be skewed towards heavy fuels, which is predicted to be driven by growth in the commercial transportation sector. Currently, the commercial transportation sector is dominated by compression ignition (CI) engines operating on diesel fuel, where the combustion is principally mixing-controlled. This mode of combustion, commonly referred to as conventional diesel combustion (CDC), is preferred in medium- and heavy-duty applications due to the difficulty of scaling spark-ignited (SI) combustion strategies to large displacement volumes and due to the efficiency advantages of the lean operation and the use of a high compression ratio in CI strategies.

As emissions regulations and fuel consumption limits become more stringent, the need to make engines more efficient without producing greater quantities of tailpipe

emissions has been at the forefront of engine development efforts across manufacturers. One of the major sources of wasted fuel energy remains heat transfer to the coolant; for a modern heavy-duty engine, this represents 20% of fuel energy that did not go toward producing work [2].

Thermal barrier coatings (TBCs) have been considered a promising way to reduce this wasted energy for more than three decades. TBCs were initially studied in gas turbine and aircraft engines, where they are used to protect the internally cooled blades from melting due to the higher operating gas temperatures. Most modern aircraft use Physical Vapor Deposition (PVD) to deposit yttria-stabilized zirconia (YSZ) coatings on many components, including combustors, augmenters and turbine blades [3]. Traditional YSZ coatings consist of an outer and inner coating. The outer coating is usually zirconium oxide, which is attractive due to its extremely low thermal conductivity and is applied by plasma-spraying and yttria is used to structurally stabilize it and prevent phase transformations that would not allow the TBC to function well. The bond coating is typically made of

NiCrAlY alloy and is expected to protect the structure from oxygen diffusion and provide strain compliance between the metal substrate and the outer coating.

Their use in internal combustion engines is motivated by the same properties, but a different principle: superior efficiencies due to reduced heat losses and the potential for increased in-cylinder pressures and temperatures, while maintaining lower heat losses to the oil and coolant [4]. Many challenges exist before they can successfully be implemented in internal combustion engines. Studies have shown that the constant thermal cycling in IC engines make the mechanical load on the TBC different from the load that it would experience in a gas turbine engine, leading to far shorter lifetimes [5]. Additionally, zirconia-based TBCs have been shown to exhibit a relatively inelastic stress/strain response and to undergo hysteresis upon cyclic loading [6]. Previous work has also shown that the pattern of heating and cooling is different between gas turbines and IC engines and is sufficient to warrant the development of different materials and methods of manufacturing for each [7].

Studies of TBCs in diesel engines have shown mixed results in terms of efficiency and fuel consumption [8, 9]. Wong et al. [10] performed simulations of YSZ TBCs with varying thicknesses and found that thin coatings gave better gains in brake thermal efficiency (BTE). Osawa et al. [11] showed that thin ceramic coatings applied to the liner of an aluminum diesel engine improved fuel consumption by 10% while causing higher exhaust and cylinder head temperatures. The reason for the improved performance is attributed to the low thermal capacitance of a thin coating, which in turn allows the wall temperature to ‘swing’ as the gas temperatures vary. This capability allows the temperature gradient to stay lower throughout, causing a reduction in heat rejection.

Toyota released a production application of a silica-reinforced porous anodized aluminum (SiRPA) temperature swing coating, which has a low heat capacity and low thermal conductivity while also being reliable in engine operation [12, 13]. Wakisaka et al. [14] showed a reduction in heat loss and a small increase in thermal efficiency when the SiRPA coating was applied to a single-cylinder DI diesel engine.

Andruskiewicz et al.[15] built a thermal wall temperature swing model using finite difference (FD) methods to capture the transient effects of various material properties and concluded that significant efficiency benefits due to both reduced work during the compression stroke and improved energy extraction during the power stroke. In another study, Andruskiewicz et al. [16] concluded that there are substantial negative effects caused by the higher porosity and surface roughness of TBCs, including trapped fuel that burns later in the cycle as well as increased heat loss at near-TDC combustion phasing. This was also supported by earlier studies by Tree et al. [17].

YSZ coatings have been shown to undergo sintering above 1200°C, which is undesirable because the particles being sprayed on coalesce without melting to form a stiff outer coating that warps the underlying substrate. Mahade et al. [18] developed a new multi-layered TBC using gadolinium zirconate (GZ) sprayed using a Suspension Plasma Spray (SPS) technique. They showed that lower thermal conductivity and improved thermal cyclic fatigue life can be obtained with the multilayered (GZ/YSZ) TBC approach compared to a

single-layer YSZ. Somhorst et al. [19] used these coatings to show that GZ/YSZ coatings had lower heat losses and higher efficiencies. They also noted that the spray-wall interaction in the TBCs was markedly different than the spray-wall interaction in the uncoated piston. They hypothesize that this may be due to the porosity acting as a crevice volume; they supported this hypothesis by showing that the spray-wall interactions of the GZ/YSZ piston and the uncoated piston became more similar when the GZ/YSZ piston was surface-sealed with Durazane. In another study, Somhorst et al. [20] also showed that soot deposits on TBC pistons play an important role in determining heat transfer. This conclusion was supported by the work of Mendera et al. [21], who showed that the ability of soot to absorb thermal radiation and subsequently reradiate that to the underlying TBC resulted in the TBC being hotter and, therefore, reduced the heat transfer to the walls.

A new generation of temperature swing coatings was recently developed by Andrie et al. [22] that simultaneously possess significantly lower thermal conductivities and heat capacities than YSZ coatings. They studied two binder materials, metal phosphate (referred to in their work as the PC) and organic polysilazane (referred to in their work as the RC). When utilized in a small, high compression ratio, spark-ignition engine, they showed overall reduction in heat rejection and a corresponding increase in the brake thermal efficiency.

Numerical analysis of coated engines has typically relied on either FD solutions, which require a high grid density near the surface to accurately predict cycle-resolved wall-temperature variation [23], or thermal resistance network solutions, which are not of sufficient fidelity to make accurate predictions for engine development and optimization applications [10, 24-27]. There are two main drawbacks associated with the finite difference approach versus analytical methods. First, the time step in a finite difference approach must be chosen to ensure numerical stability, and second and most important, all the nodal temperatures are computed and stored for each time step even though only the surface node is the output of interest explicitly for providing boundary conditions in engine simulation.

Recently, Koutsakis and co-workers developed conduction heat transfer [28-31] and durability models [32] for multi-layer engine walls. The heat transfer method enjoys several advantages over conventional finite difference approaches [31]. These include faster computational times (the Koutsakis solution was shown to be ~10,000x faster than an equivalent finite difference code) as well as guaranteed numerical stability and accuracy regardless of the overall timestep. This improvement in performance is primarily driven by the ability of the model to predict the surface temperature without calculation of any intermediate temperatures. They further coupled their solver with the commercial engine simulation software GT-POWER [33] to simulate different coatings in a 4-cylinder, 4.5L medium-duty engine and showed the ability of the model to predict heat transfer rates and in-cylinder temperatures. The durability model was experimentally verified to predict the delamination of several coated pistons that had been tested in a high-output, single-cylinder diesel engine [34]. A large-scale optimization to identify the trade-off between engine performance and coating durability over a full drive cycle has also been studied [35].

From the above review of the literature, it is clear that a need exists for testing of the new generation of thermal swing coatings in DI diesel engines to evaluate the benefits of their use compared to uncoated pistons and traditional YSZ TBCs. Additionally, the validation of numerical techniques of TBC-study would also greatly speed the development process up and allow TBCs to come to the market sooner. Accordingly, in this work, two coatings were considered for study: the first is an HVLP coating with a metal phosphate binder, while the second is a conventional YSZ coating. These were deposited on modified pistons and a thorough experimental and numerical investigation was carried out. Experiments were conducted in a medium-duty single-cylinder diesel engine. The Koutsakis wall-temperature solver was coupled with a fully calibrated single-cylinder GT-POWER model of the same engine and simulations were carried out.

Experimental Setup

Test Cell Details

The experimental work in this study was conducted in a fully instrumented test cell featuring the Cummins ISB engine, modified for single-cylinder operation. The ISB is a six-cylinder diesel engine typically found in medium-duty applications, such as pickup trucks, buses, recreational vehicles, and other vocational vehicles; the key aspects of the engine are summarized in [Table 1](#). A short description of the test cell follows; further details and a schematic of the test cell can be found in earlier works by the authors [36–39].

The engine was coupled to a Direct Current (DC) trunnion-mounted swinging fields dynamometer manufactured by GE. All the experiments in this study were steady-state, with speed being fixed by controlling the dynamometer, which was used both to load the engine and to drive it when the engine was not being fueled (commonly referred to as ‘motoring’ the engine).

A National Instruments (NI) ECS-1002 cart, fitted with a PXI® chassis was used for high-speed data acquisition and control. High-speed data was obtained with a resolution of 0.1 Crank Angle Degrees (CAD), synchronized to a BEI optical encoder that records the crankshaft position. In-cylinder pressure was measured by a water-cooled Kistler 6067

piezoelectric pressure transducer and recorded over 500 cycles. This ‘raw’ pressure signal was then filtered using a Gaussian roll-off filter, which uses a Nyquist frequency adjusted according to the engine speed. The net Heat Release Rate (nHRR) was then calculated in the method of Gatowski et al. [40] for each pressure signal and then averaged. The nHRR data was visually checked before and after filtering of the pressure data to ensure that any features removed through filtering were of lesser magnitude than the features of interest in this study.

K-type thermocouples and pressure transducers were also strategically placed throughout the test cell, including in the cooling, intake, exhaust, fuel, and oil systems to ensure that the test cell was functioning appropriately. Intake pressure was set by using a QB2 pressure controller and exhaust pressure was set independently by throttling. Surge tanks were placed upstream of the intake runner and downstream of the exhaust runner to smooth out the instantaneous variations in pressure and flow rate that are expected in a single-cylinder test cell. Heaters were provided on the intake air and coolant streams to allow the intake air and coolant temperatures to be precisely regulated. The oil system used in this study was the one found on the stock engine and thus, oil temperature was not regulated in this manner, although it was seen to closely match the coolant temperature, which was maintained at 90°C for the entirety of this work.

The fuel temperature was externally regulated to 25°C and the injection pressure was maintained within ±2 bar for the cases reported in this study. Fuel flow was measured by using an Endress and Hauser Promass A83 Coriolis flowmeter.

Low-speed data was collected using an NI CompactDAQ chassis, with 500 cycles of data collected and averaged for each data point in this work. The low-speed data collection was precisely synced with the high-speed data collection using an instance of the NI LabVIEW Shared Variable Engine.

Gaseous emissions were measured by using a Thermo Nicolet Nexus 670 Fourier Transform Infrared (FTIR) spectrometer coupled to a Real-Time Exhaust Gas Analysis (REGA) sampling cart. The exhaust gas was transported to the emissions bench in a heated sample line, which maintained the exhaust gas at 185 °C; this was done to ensure that no moisture/hydrocarbons condense out, so that all the emissions measurement would be performed on a wet basis. A Nicolet® 2m gas cell with gold plated mirrors and Zinc Selenide (ZnSe) windows was used to continuously sample the gas and the software package Omnic® was used to collect and process data continuously. All the heated components in the REGA cart were maintained at 185 °C to ensure that the temperature of the gas entering the gas cell (a parameter to which the instrument is very sensitive) was at 185 °C. The pressure in the cell was maintained at 650 Torr. A highly sensitive, liquid-N₂-cooled Mercury Cadmium Telluride - A (MCT/A) detector was used to compensate for the attenuation caused by the internal reflections in the gas cell and the FTIR was set to coadd 8 sub-samples to give each sample; this ensured maximum signal-to-noise ratio while minimizing the response time. The sample was quantified by a Classical Least Squares (CLS) technique, using reference spectra from a comprehensive library of exhaust gas spectra in a customized quantification method to ensure that the final result did not omit any significant constituents of the exhaust.

TABLE 1 Details of medium-duty engine used in this study.

Parameter	Value(s)
Engine	2013 Cummins 6.7 L ISB
Configuration:	Inline six-cylinder converted to single-cylinder operation
Displacement per cylinder [L/cyl]:	1.1
Bore [mm]	106.9
Stroke [mm]	124
Compression Ratio:	17.3
High-Pressure Common Rail (HPCR) Pump	Bosch CP3 (externally driven by 5 HP electric motor)

An emissions-based AFR was calculated based on the measured emissions in the method of Dempsey [41] and compared to the mass-based AFR (calculated as the ratio of the measured air and fuel mass flow rates); a data point was rejected if these two values of AFR do not lie within 5 percent of each other. Oxygen concentration was measured by using a wideband O₂ sensor from Robert Bosch GmbH and an approximate air-fuel ratio (AFR) was calculated from this using calibration curves supplied by Bosch. This value of AFR was intended to serve as a sanity check on the more precise mass- and emissions-based measures of AFR.

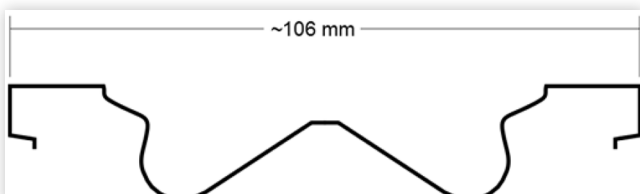
Particulate emissions were measured by using an AVL 415 SE smokemeter, which works on the principle of filter paper blackening [42]. A sampling volume of 1000 mL was used for the particulate measurement, and 5 samples were collected and averaged for each data point.

Piston Details

In its stock configuration, the ISB engine uses cast aluminum pistons with a stepped lip bowl design, which has been shown to help distribute fuel between the bowl and squish regions when the spray is appropriately targeted, helping to improve oxygen utilization and minimize sooting [43]. A schematic of the piston profile used in this study is shown in Figure 1.

Two coatings were chosen for study in this work. The first is an HVLP coating with a metal phosphate binder. This coating was an improved version of the PC coating used by Andrie et al [22], with lower surface roughness and density values, and is referred to as the SPC. The SPC is cured at a temperature around 200 °C, which makes it well-suited to be used with aluminum components, such as the piston used in this study. The second coating chosen for study is a conventional YSZ coating with a single bond layer. The properties of the coating materials are given in Table 5. For the coated pistons, the thicknesses of the coatings (and the bond material, in the case of the YSZ-coated piston) was compensated for by first removing a layer of aluminum from the surface of the pistons. The volumes of the uncoated piston bowl and those of the coated piston bowls were compared afterward to ensure that the coating process did not affect the displacement and/or the compression ratio. During the experimentation, the piston rings were reused between the pistons to shorten the break-in time; the pistons were operated for 15 hours prior to the collection of the data described here.

FIGURE 1 Piston profile for 2013 Cummins ISB 6.7.



Fuel Injector Details

A Bosch CRI2-16 solenoid injector was used in this study and the characteristics of the injector are shown in Table 2. The fuel injector was driven using a 75 V back boost voltage with an opening current of 20 A for 300 µs and a 14 A hold current for the remaining length of the injection duration.

Fuel Details

Commercially available on-highway low-sulfur diesel fuel was used for all the experiments and the key properties are listed in Table 3.

Numerical Model

A baseline/uncoated model of the single-cylinder engine was constructed in GT-POWER and validated; the details of this validation were documented in a previous study [44]. The Koutsakis solver was then integrated into the model. This tool accommodates the multilayer conduction heat transfer physics which takes place in an internal combustion engine environment. The mathematical solution relies on complex analysis to invert the Laplace transform from the frequency back to the time domain. The time-response functions X_o and Y_o are required to be calculated only once before the simulation initiates. The former response refers to the temperature rise due to a heat flux q'' at the combustion surface while the latter response refers to a temperature change due to temperature t_c at the coolant/oil surface. The superposition of the two previous subproblems which are convolved the information from both surfaces to determine the instantaneous wall surface temperature $t_{o,wall}$ for a multilayer wall as:

$$t_{o,wall} = X_o \otimes q'' + Y_o \otimes t_c$$

TABLE 2 Fuel injector details.

Parameter	Actual
Injector Family	Bosch CRI2-16
Number of Orifices	8
Orifice Diameter [µm]	138
Orifice Included Angle	145°
Nozzle Fuel Passage Length [mm]	0.95
Rated Flow @ 100 bar [cm ³ /30s]	500
C _d - Discharge Coefficient [-]	0.86
k _s - Rounding Factor [-]	1.3

TABLE 3 Properties of diesel fuel used in this study.

Parameter	Value
Cetane Number	45
Density [kg/m ³]	857
Lower Heating Value [MJ/kg]	42.78
H-C ratio	1.78
O-C Ratio	0

where the symbol \otimes denotes convolution. Further details about the heat transfer model, including equations and explanations may be found in [31].

Methods

Experimental Methods

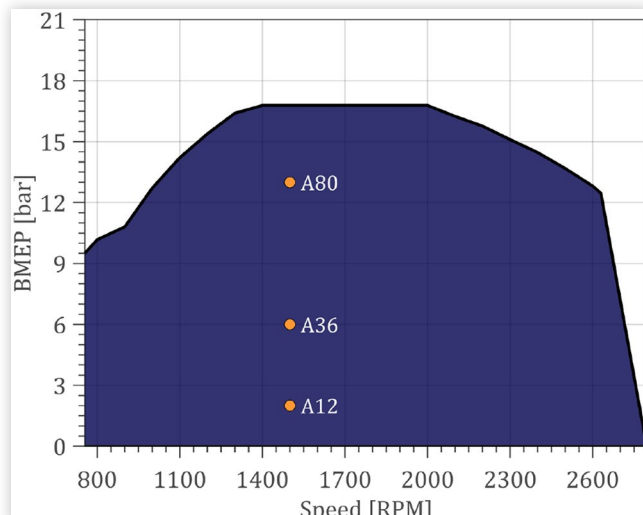
The ISB engine's peak operating line is shown in Figure 2. The A, B and C speeds were calculated using this peak operating line according to the conventions set forth in 40 CFR § 1065.610 [45] to be 1500, 1900 and 2300 revolutions per minute (RPM), respectively. The A speed was chosen for study and three operating points corresponding to 12, 36 and 80 % of peak load in the six-cylinder engine were chosen for study. These chosen points are labeled 'A12', 'A36' and 'A80', respectively and are shown on the engine's operating map in Figure 2.

Operating parameters that are representative of the stock engine calibration are chosen at each point; however, the injection schedule is modified to be single-injection, to simplify the analysis and eliminate any confounding effects a multi-injection schedule may have on the results. The final parameters at each point are described in Table 4.

An SOI sweep was conducted at each point, to consider the effects of combustion phasing, within the following limitations:

- Maximum combustion instability of 5% COV(GIMEP),
- Maximum exhaust runner temperature of 550 °C,
- Maximum peak pressure rise rate (PPRR) of 25 bar/CAD,
- Maximum peak cylinder pressure (PCP) of 180 bar,
- Minimum AFR of 19,
- Maximum fsNOx emission of 60 g/kg_{fuel},
- Maximum soot emission of 2 FSN.

FIGURE 2 Points chosen for study, shown on the operating map of the ISB engine.



Numerical Methods

Experimentally measured boundary conditions such as intake pressure, injection pressure, etc. were input to the GT-POWER as boundary conditions. An overall/global multiplier to the convection heat transfer coefficient of the Woschni model in GT-POWER was adjusted until a close match was obtained between the cylinder pressure predicted by the model for the uncoated piston and the experimentally measured results for the uncoated piston. This value of the heat transfer multiplier was used across all the pistons, operating points and SOI timings studied in this work. The thicknesses, densities, conductivities, and heat capacities of the piston coatings as well as properties of the aluminum "substrate", the cylinder head and the cylinder liner were input to the Koutsakis solver as boundary conditions; these are summarized in Table 5.

Additionally, the surface temperatures of the piston, cylinder head and cylinder liner on the backsides were input as boundary conditions. The backside surface temperatures were set based on preliminary finite element analysis using the experimentally measured oil and coolant temperatures at the studied points and are given in Table 6. These values are seen to be consistent with direct measurements and CFD found in the literature [46-48] as well.

TABLE 4 Parameters for chosen operating conditions.

Parameter	A12	A36	A80
Engine Speed [RPM]	1500		
Nominal GIMEP [bar]	4	8	15
Intake Pressure [kPa]	130	150	190
Exhaust Pressure [kPa]	175	200	220
Intake Temperature [°C]	50		
Injection Schedule	Single-injection		
SOI timing [°ATDC]	Swept		
Injection Quantity [mg/cycle]	23	44	85
AFR [-]	47	29	20
EGR Rate [%]	20	18	15
Injection Pressure [bar]	950	1300	1500

TABLE 5 Properties of materials used in the Koutsakis solver.

Value	Thickness [mm]	Density [kg/m ³]	Specific Heat [J/kg-K]	Thermal Cond. [W/m-K]
Cylinder Head (Gray Iron)	10.6	7879	507	49
Cylinder Liner (Cast Iron)	5.5	7870	500	61
Piston (Aluminum Alloy)	13 ¹	2702	949	140
SPC Coating	0.15	350	1400	0.31
YSZ Coating	0.15	3830	574	1.7
YSZ Bond Layer	0.1	4290	536	2.72

¹ Consistent with the experiments, aluminum thickness was reduced to keep total piston thickness constant, when simulating the coated cases

TABLE 6 Backside cylinder head, cylinder liner and piston temperatures used as boundary conditions for the Koutsakis solver at each of the chosen operating conditions.

Parameter	A12	A36	A80
Cylinder Head Backside Temperature [°C]	150	180	210
Cylinder Liner Backside Temperature [°C]	110	125	140
Piston Backside Temperature [°C]	140	180	220

Results

Experimental Results - A12 (Low Load)

At the low load condition, it was observed that the most advanced SOI was imposed by the NOx limit, while the most retarded SOI was constrained by the stability limit. Comparisons of GIE, EGT, fsNOx emissions and soot

FIGURE 3 Clockwise from top left: comparisons of GIE, EGT, fsNOx emissions and soot emissions amongst the uncoated, SPC and YSZ-coated pistons at the A12 condition.

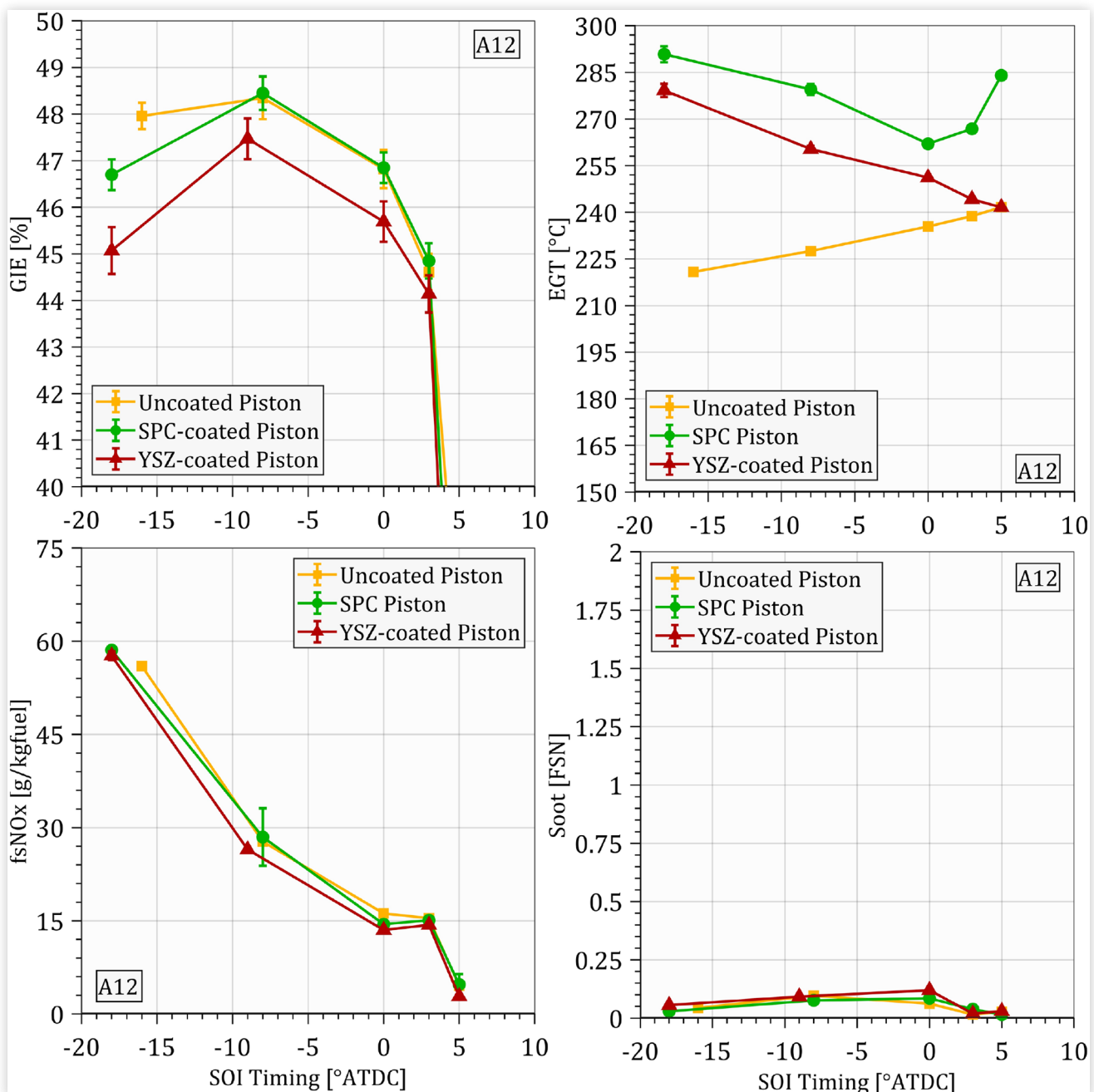
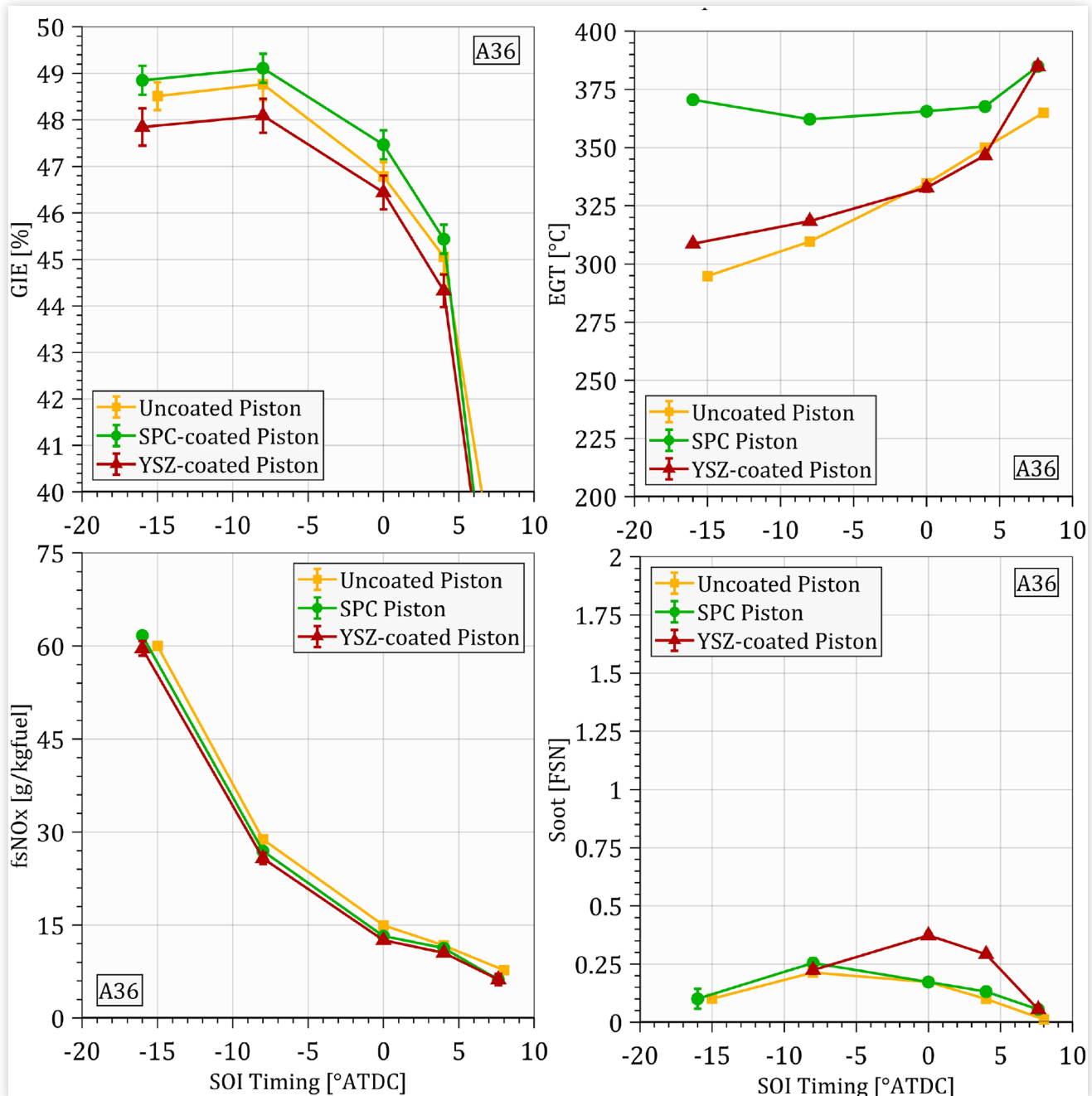


FIGURE 4 Clockwise from top left: comparisons of GIE, EGT, fsNOx emissions and soot emissions amongst the uncoated, SPC and YSZ-coated pistons at the A36 condition.

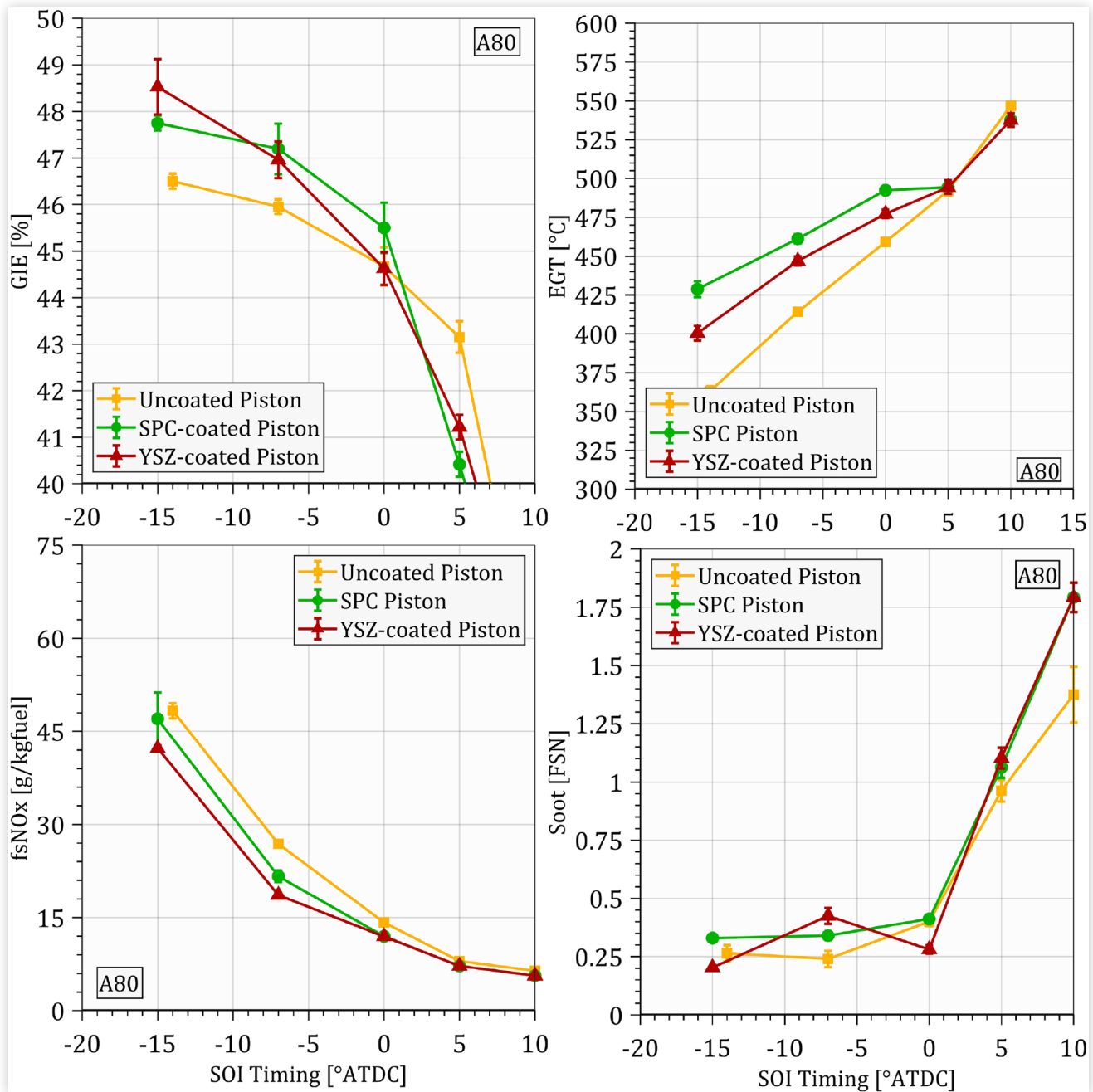


emissions amongst the different pistons at the A12 condition are shown in Figure 3. It is seen that the SPC-coated piston offers no efficiency benefit at this condition, although an efficiency loss is incurred by using the YSZ-coated piston. However, there is an EGT benefit to using both the SPC-coated and the YSZ-coated pistons at this condition. This EGT benefit is of particular significance at this condition due to the well-known difficulty of aftertreatment thermal management when operating at low loads [49, 50]. No soot or NOx penalty is observed when using the coated pistons.

Experimental Results - A36 (Medium Load)

At the medium load condition also, it was observed that the most advanced SOI was imposed by the NOx limit, while the most retarded SOI was constrained by the stability limit. Comparisons of GIE, EGT, fsNOx emissions and soot emissions amongst the different pistons at the A36 condition are shown in Figure 4. No statistically significant differences in efficiency are observed amongst the pistons at the A36

FIGURE 5 Clockwise from top left: comparisons of GIE, EGT, fsNOx emissions and soot emissions amongst the uncoated, SPC and YSZ-coated pistons at the A80 condition.



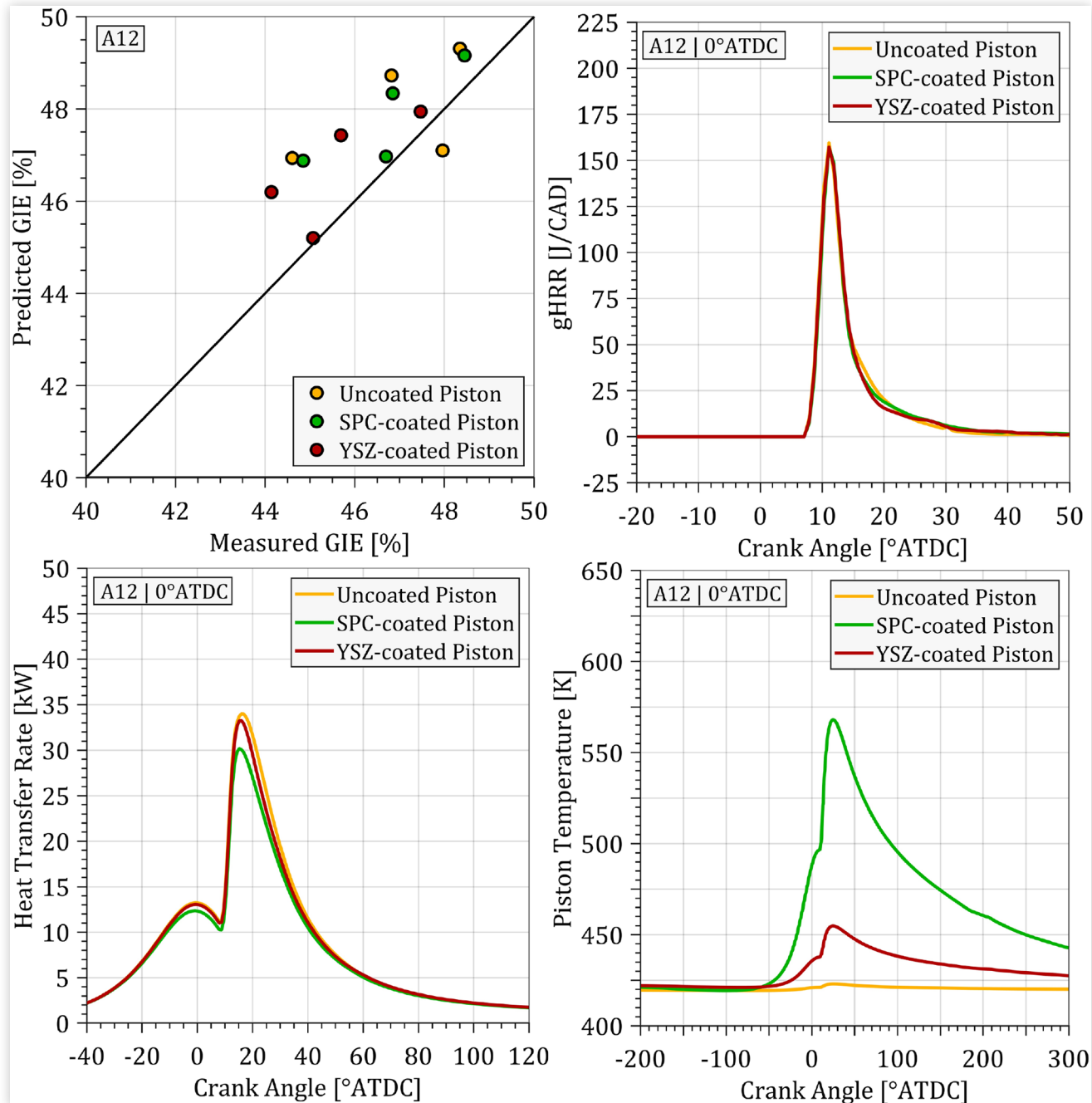
condition. However, the EGT benefit to using the SPC-coated piston continues to be present at this condition. No NOx penalty is observed when using the coated pistons, and a slight soot penalty is observed when using the YSZ-coated piston.

Experimental Results - A80 (High Load)

At the high load condition, the most advanced SOI was constrained by the PCP limit, while the most retarded SOI was imposed by the EGT limit. Comparisons of GIE, EGT,

fsNOx emissions and soot emissions amongst the different pistons at the A80 condition are shown in Figure 5. At the A80 condition, an increase in efficiency is observed when using the SPC-coated piston. This benefit is seen to be highest at the earliest SOI timing; the YSZ-coated and SPC-coated piston are seen to have equal efficiencies at the earliest SOI timing, although the YSZ-coated piston's efficiency is seen to drop off quickly as the SOI timing is retarded. Additionally, the EGT benefit to using the SPC-coated piston continues to be present at this condition. Once again, no soot or NOx penalty is observed when using the coated pistons.

FIGURE 6 Top Left: comparisons of predicted and measured GIE at the A12 condition; Clockwise from Top Right: comparison of gHRRs, heat transfer rates and piston surface temperatures amongst the uncoated, SPC and YSZ-coated pistons at the A12 condition with an SOI timing at 0 °aTDC.

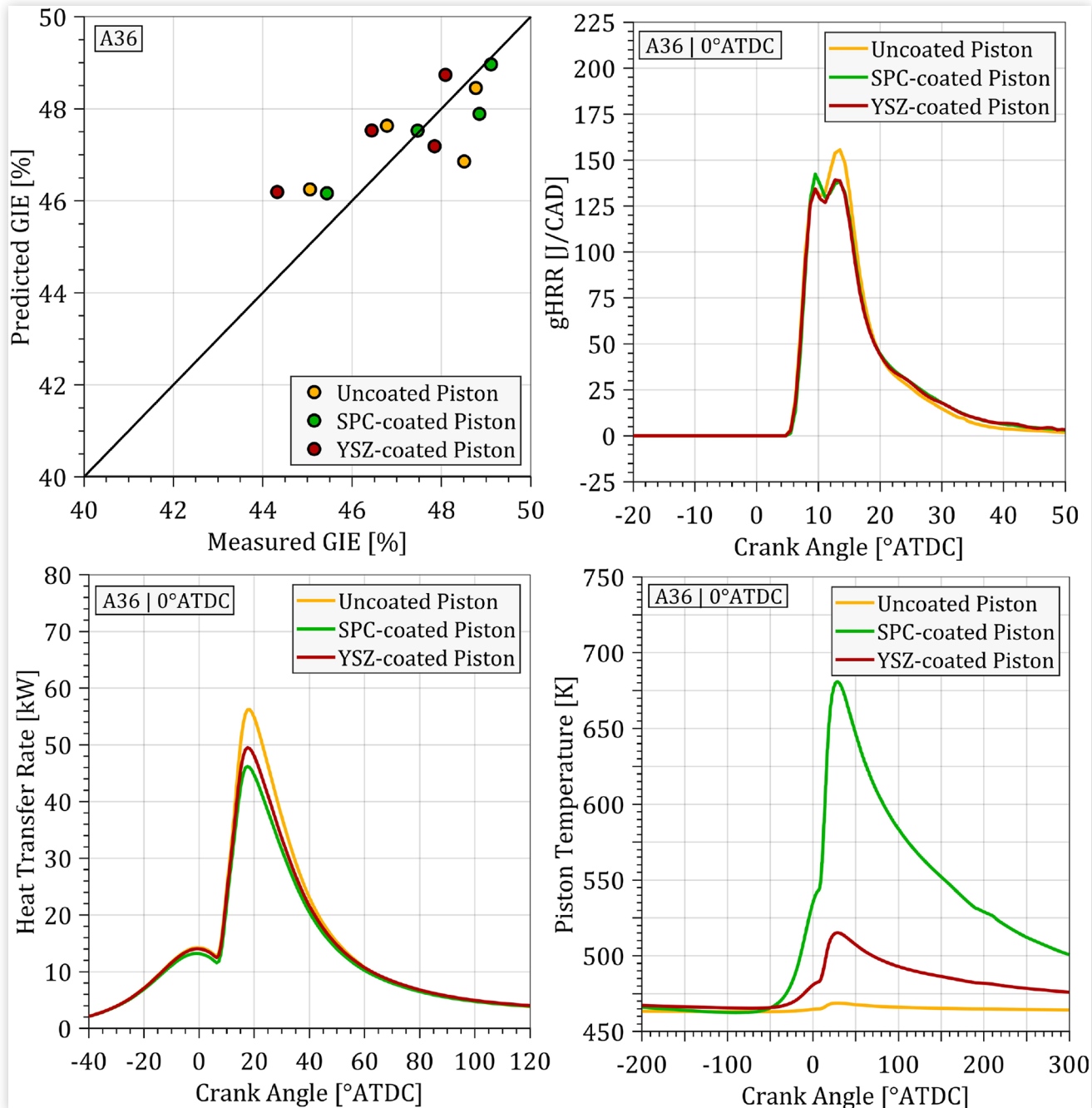


Modeling Results - A12 (Low Load)

Figure 6 shows the results of the GT-POWER modeling at the low-load. The top left plot shows the quality of the GIE predictions at the low-load condition. The data is primarily separated by piston, with each circle of a given color representing one SOI timing; it is seen that the model is able to reproduce the efficiencies measured in the test cell faithfully. The gross heat

release rates (gHRRs), which are the heat release rates from the chemical reactions, predicted by the model are shown in the top right plot; it is seen that the differences in the gHRRs between the pistons are minimal at this condition, which suggests that any differences seen in the GIE and EGT between the pistons are due to differences in the heat transfer rates. The predicted piston temperature variations during the cycle are shown in the bottom right plot. It is seen that the temperature of the uncoated piston remains almost invariant during

FIGURE 7 Top Left: comparisons of predicted and measured GIE at the A36 condition; Clockwise from Top Right: comparison of gHRRs, heat transfer rates and piston surface temperatures amongst the uncoated, SPC and YSZ-coated pistons at the A36 condition with an SOI timing at 0 °aTDC.



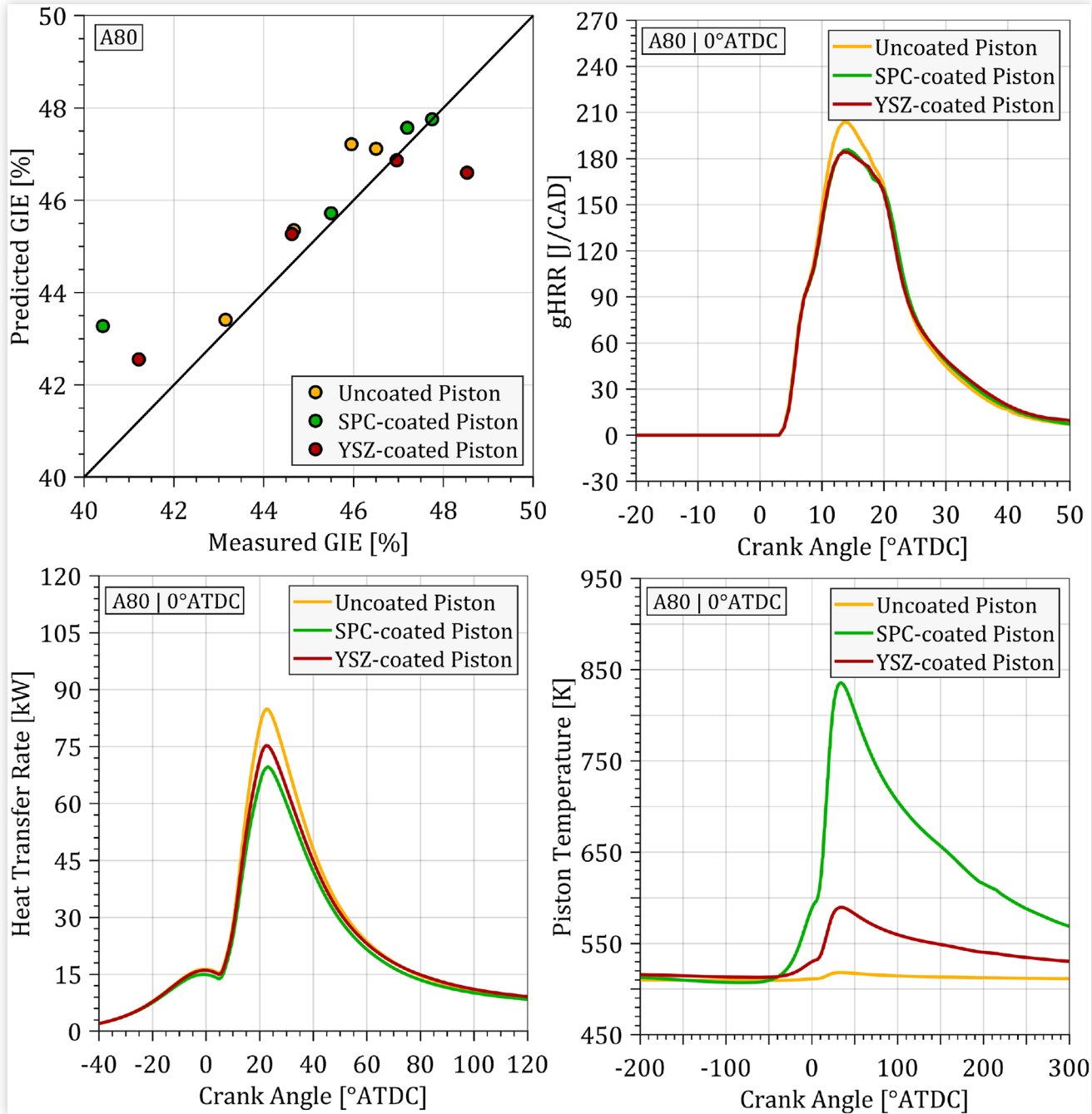
the cycle, while the YSZ-coated piston has a minimal temperature swing; the SPC-coated piston is seen to have a temperature swing that is almost an order of magnitude higher than the YSZ-coated piston. Finally, the bottom left plot shows the heat transfer rates and it is seen that, as might be expected based on the piston surface temperature variation, the SPC-coated piston has the least heat transfer, followed by the YSZ-coated piston, followed by the uncoated piston. This trend in heat transfer, taken in conjunction with the trends in GIE and EGT observed in Figure 3, suggests that the improved conductivity and heat capacity of the coated pistons is

translating into higher EGTs, but not higher GIEs at the A12 condition. Additionally, it is seen that the SPC-coated piston has a lower heat transfer rate prior to SOI, while no such difference is observed with the YSZ-coated and uncoated pistons.

Modeling Results - A36 (Medium Load)

Figure 7 shows the results of the GT-POWER modeling at the medium-load. The top left plot shows the quality of the GIE

FIGURE 8 Top Left: comparisons of predicted and measured GIE at the A80 condition; Clockwise from Top Right: comparison of gHRRs, heat transfer rates and piston surface temperatures amongst the uncoated, SPC and YSZ-coated pistons at the A80 condition with an SOI timing at 0 °aTDC.



predictions at the medium-load condition, separated by piston; once again, it is seen that the model is able to reproduce the efficiencies measured in the test cell faithfully. The gHRRs predicted by the model are shown in the top right plot; it is seen that the differences in the gHRRs between the pistons are minimal at this condition also. The predicted piston temperature variations during the cycle are shown in the bottom right plot. The trends seen at the A12 condition are seen here as well: the temperature of the uncoated piston remains almost invariant during the cycle, while the

YSZ-coated piston has a minimal temperature swing; the SPC-coated piston is seen to have a temperature swing that is almost an order of magnitude higher than that of the YSZ-coated piston. Finally, the bottom left plot shows the heat transfer rates and it is seen that the SPC-coated piston has the least heat transfer, followed by the YSZ-coated piston, followed by the uncoated piston. This suggests that, at the A36 conditions also, the improved conductivity and heat capacity of the SPC-coated piston is translating into lower heat transfer rates, but the additional in-cylinder energy is then increasing the

EGTs, but not the GIEs, as was previously observed in [Figure 4](#). It is also seen that the SPC-coated piston has a lower heat transfer rate prior to SOI, while the YSZ-coated and uncoated pistons continue to have identical heat transfer rates prior to SOI.

Modeling Results - A80 (High Load)

[Figure 8](#) shows the results of the GT-POWER modeling at the high-load. The top left plot shows the quality of the GIE predictions at the high-load condition, separated by piston; once again, it is seen that the model is able to reproduce the efficiencies measured in the test cell faithfully. The gHRRs predicted by the model are shown in the top right plot; it is seen that the differences in the gHRRs between the pistons are minimal at this condition also. The predicted piston temperature variations during the cycle are shown in the bottom right plot. The trends seen at the A12 and A36 conditions are seen here as well: the temperature of the uncoated piston remains almost invariant during the cycle, while the YSZ-coated piston has a minimal temperature swing; the SPC-coated piston is seen to have a temperature swing that is 300 K greater than that of the YSZ-coated piston. Finally, the bottom left plot shows the heat transfer rates and it is seen that the SPC-coated piston has the least heat transfer, followed by the YSZ-coated piston, followed by the uncoated piston. This suggests that, at the A80 conditions also, the improved conductivity and heat capacity of the SPC-coated piston is translating into lesser heat transfer; however, at the A80 condition, this translates into both increased GIE and an increased EGT, as was previously observed in [Figure 5](#). It is also seen that the SPC-coated piston has a lower heat transfer rate prior to SOI, while the YSZ-coated and uncoated pistons continue to have identical heat transfer rates prior to SOI.

Summary and Conclusions

In summary, a low-conductivity, low-heat capacity thermal barrier coating was studied in a medium-duty single-cylinder diesel engine alongside a conventional plasma-sprayed, Yttria-stabilized zirconia (YSZ) coating. Low-, medium-, and high-load operating conditions were chosen at a single speed and sweeps of injection timing were conducted. Variations of gross indicated efficiency (GIE), exhaust gas temperature (EGT) and criteria pollutant emissions as injection timing was varied were reported. A calibrated GT-POWER model of the single-cylinder engine was modified to use an analytical wall temperature model developed by Koutsakis et al. [28-30] and simulations were carried out. Predictions of the piston surface temperatures alongside gross Heat Release Rates and heat transfer rates were obtained from the model and reported. The key observations and conclusions from the study are summarized below.

1. It was observed that the SPC coating offered a 1-1.5% improvement in GIE at the high-load operating condition.

2. Improvements were observed in EGT when using both the YSZ-coated and SPC-coated piston at all three operating conditions.

This result is of particular significance when considering the well-known difficulties of keeping after-treatment warm when operating at low-loads, which is critical to minimizing criteria pollutant emissions.

3. No emissions penalty was seen when operating using either the SPC- or YSZ-coated pistons at any of the operating conditions studied here, compared to the uncoated piston.
4. Reliable operation of the SPC coating was confirmed on a CI engine environment over 25 hours of testing.
5. After calibrating the GT-POWER Woschni heat transfer model to reproduce the experimental results of the uncoated piston, the predictions for the SPC-coated piston and the YSZ-coated piston were seen to be faithful to the experimental data as well.
6. Using the predictions from the Koutsakis wall-temperature solver, the dramatic increase in temperature swing expected from the lowering of the thermal conductivity and heat capacity in the SPC coating was confirmed.
7. The heat transfer rates predicted by the model confirmed the experimental GIE results and suggested that the reduction in conductivity and heat capacity of the coatings increases the in-cylinder energy. However, this increase is primarily reflected as an increase in exhaust enthalpy and as an increase in GIE only secondarily.

Thus, it was found that advantages to using the SPC-coated pistons existed at all the conditions studied, showcasing the promise of low-conductivity, low-heat capacity coatings in developing higher efficiency diesel engines in the future.

Acknowledgements

The experimental work was funded in part by the Advanced Research Projects Agency-Energy (ARPA-E), U.S. Department of Energy under Award Number DE-AR0000600. The views and opinions of authors expressed herein do not necessarily state or reflect those of the United States Government or any agency thereof. The authors would also like to thank the Direct-injection Engine Research Consortium (DERC) [51] for partially funding the experimental portion of this work, Cummins Inc. for donating the engine used in this study and Adiabatics Inc. for manufacturing the coated pistons. The authors would like to thank John Deere Power Systems for funding the research into the Koutsakis wall temperature solver. The authors would also like to thank Dr.-Ing Philippe Leick of Robert Bosch GmbH for his assistance with the selection of a suitable nozzle for the fuel injector used in this study. The authors would also like to thank Joshua Leach, the Senior Systems Administrator of the Center for his invaluable assistance with setting up and running the GT-POWER simulations seamlessly in spite of the massive disruption caused by the worldwide COVID-19 pandemic to research activities.

References

1. ExxonMobil. "The Outlook on Energy: a View to 2040," 2019.
2. Thiruvengadam, A. et al., "Characterization of Energy Distribution and Efficiency in a Modern Heavy-Duty Diesel Engine," *SAE Int. J. Engines* 13, no. 4 (2020), doi:[10.4271/03-13-04-0037](https://doi.org/10.4271/03-13-04-0037).
3. Meier, S.M. and Gupta, D.K., "The Evolution of Thermal Barrier Coatings in Gas Turbine Engine Applications," *J. Eng. Gas Turbines Power* 116, no. 1 (1994): 250-257, doi:[10.1115/1.2906801](https://doi.org/10.1115/1.2906801).
4. Jaichandar, S. and Tamilporai, P., "Low Heat Rejection Engines - An Overview," SAE Technical Paper [2003-01-0405](#) (2003). <https://doi.org/10.4271/2003-01-0405>.
5. Beardsley, M.B., "Potential Use of Quasicrystalline Materials as Thermal Barrier Coatings for Diesel Engine Components," Ph.D. Thesis, Materials Science and Engineering, Iowa State University, Ames, IA, 2008.
6. Wesling, K.F., Socie, D.F., and Beardsley, B., "Fatigue of Thick Thermal Barrier Coatings," *J. Am. Ceram. Soc.* 77, no. 7 (1994): 1863-1868, doi:[10.1111/j.1151-2916.1994.tb07063.x](https://doi.org/10.1111/j.1151-2916.1994.tb07063.x).
7. Nelson, W.A. and Orenstein, R.M., "TBC Experience in Land-Based Gas Turbines," *J. Therm. Spray. Tech.* 6 (1997): 176-180, doi:[10.1007/s11666-997-0009-5](https://doi.org/10.1007/s11666-997-0009-5).
8. Bryzik, W. and Kamo, R., "TACOM/Cummins Adiabatic Engine Program," SAE Technical Paper [830314](#) (1983). <https://doi.org/10.4271/830314>.
9. Woschni, G., Spindler, W., and Kolesa, K., "Heat Insulation of Combustion Chamber Walls — A Measure to Decrease the Fuel Consumption of I.C. Engines?" SAE Technical Paper [870339](#) (1987). <https://doi.org/10.4271/870339>.
10. Wong, V.W., Bauer, W., Kamo, R., Bryzik, W. et al., "Assessment of Thin Thermal Barrier Coatings for I.C. Engines," SAE Technical Paper [950980](#) (1995). <https://doi.org/10.4271/950980>.
11. Osawa, K., Kamo, R., and Valdmanis, E., "Performance of Thin Thermal Barrier Coating on Small Aluminum Block Diesel Engine," SAE Technical Paper [910461](#) (1991). <https://doi.org/10.4271/910461>.
12. Kawaguchi, A., Iguma, H., Yamashita, H., Takada, N. et al., "Thermo-Swing Wall Insulation Technology; - A Novel Heat Loss Reduction Approach on Engine Combustion Chamber," SAE Technical Paper [2016-01-2333](#) (2016). <https://doi.org/10.4271/2016-01-2333>.
13. Kosaka, H. et al., "Concept of "Temperature Swing Heat Insulation" in Combustion Chamber Walls, and Appropriate Thermo-Physical Properties for Heat Insulation Coat," *SAE Int. J. Engines* 6, no. 1 (2013): 142-149, doi:[10.4271/2013-01-0274](https://doi.org/10.4271/2013-01-0274).
14. Wakisaka, Y. et al., "Reduction of Heat Loss and Improvement of Thermal Efficiency by Application of "Temperature Swing" Insulation to Direct-Injection Diesel Engines," *SAE Int. J. Engines* 9, no. 3 (2016): 1449-1459, doi:[10.4271/2016-01-0661](https://doi.org/10.4271/2016-01-0661).
15. Andruskiewicz, P., Najt, P., Durrett, R., Biesboer, S. et al., "Analysis of the Effects of Wall Temperature Swing on Reciprocating Internal Combustion Engine Processes," *Int. J. Eng. Res.* 19, no. 4 (2017): 461-473, doi:[10.1177/1468087417717903](https://doi.org/10.1177/1468087417717903).
16. Andruskiewicz, P., Najt, P., Durrett, R., and Payri, R., "Assessing the Capability of Conventional In-cylinder Insulation Materials in Achieving Temperature Swing Engine Performance Benefits," *Int. J. Eng. Res.* 19, no. 6 (2017): 599-612, doi:[10.1177/1468087417729254](https://doi.org/10.1177/1468087417729254).
17. Tree, D.R., Wiczynski, P.D., and Yonushonis, T.M., "Experimental Results on the Effect of Piston Surface Roughness and Porosity on Diesel Engine Combustion," SAE Technical Paper [960036](#) (1996). <https://doi.org/10.4271/960036>.
18. Mahade, S., Curry, N., Björklund, S., Markocsan, N. et al., "Thermal Conductivity and Thermal Cyclic Fatigue of Multilayered Gd₂Zr₂O₇/YSZ Thermal Barrier Coatings Processed by Suspension Plasma Spray," *Surf. Coat. Technol.* 283 (2015): 329-336, doi:[10.1016/j.surfcoat.2015.11.009](https://doi.org/10.1016/j.surfcoat.2015.11.009).
19. Somhorst, J., Uczak De Goes, W., Oevermann, M., and Bovo, M., "Experimental Evaluation of Novel Thermal Barrier Coatings in a Single Cylinder Light Duty Diesel Engine," SAE Technical Paper [2019-24-0062](#) (2019). <https://doi.org/10.4271/2019-24-0062>.
20. Somhorst, J., Oevermann, M., Bovo, M., and Denbratt, I., "Evaluation of Thermal Barrier Coatings and Surface Roughness in a Single-Cylinder Light-Duty Diesel Engine," *Int. J. Eng. Res.* (2019), doi:[10.1177/1468087419875837](https://doi.org/10.1177/1468087419875837).
21. Mendera, K.Z., "Effectiveness of Plasma Sprayed Coatings for Engine Combustion Chamber," SAE Technical Paper [2000-01-2982](#) (2000). <https://doi.org/10.4271/2000-01-2982>.
22. Andrie, M., Kokjohn, S., Paliwal, S., Kamo, L.S. et al., "Low Heat Capacitance Thermal Barrier Coatings for Internal Combustion Engines," SAE Technical Paper [2019-01-0228](#) (2019). <https://doi.org/10.4271/2019-01-0228>.
23. Ghandhi, J. and Koutsakis, G., "Comment on "Numerical approach to define a thermodynamically equivalent material for the conjugate heat transfer simulation of very thin coating layers" by P. Olmeda, X. Margot, P. Quintero, J. Escalona, International Journal of Heat and Mass Transfer, Vol. 162 (2020) 120377," *International Journal of Heat and Mass Transfer* 173, no. 121190: 2021, doi:[10.1016/j.ijheatmasstransfer.2021.121190](https://doi.org/10.1016/j.ijheatmasstransfer.2021.121190).
24. Assanis, D.N. and Heywood, J.B., "Development and Use of a Computer Simulation of the Turbocompounded Diesel System for Engine Performance and Component Heat Transfer Studies," SAE Technical Paper [860329](#) (1986). <https://doi.org/10.4271/860329>.
25. Yao, M., Ma, T., Wang, H., Zheng, Z. et al., "A Theoretical Study on the Effects of Thermal Barrier Coating on Diesel Engine Combustion and Emission Characteristics," *Energy* 162 (2018): 744-752, doi:[10.1016/j.energy.2018.08.009](https://doi.org/10.1016/j.energy.2018.08.009).
26. Poubeau, A., Vauvy, A., Duffour, F., Zaccardi, J.-M. et al., "Modeling Investigation of Thermal Insulation Approaches for Low Heat Rejection Diesel Engines Using a Conjugate Heat Transfer Model," *Int. J. Eng. Res.* 20, no. 1 (2018): 92-104, doi:[10.1177/1468087418818264](https://doi.org/10.1177/1468087418818264).
27. Killingsworth, N., Powell, T., O'Donnell, R., Filipi, Z. et al., "Modeling the Effect of Thermal Barrier Coatings on HCCI Engine Combustion Using CFD Simulations with Conjugate

- Heat Transfer," SAE Technical Paper [2019-01-0956](#) (2019). <https://doi.org/10.4271/2019-01-0956>.
28. Koutsakis, G. and Ghandhi, J.B., "An Analytical Approach for Calculating Instantaneous Multilayer-Coated Wall Surface Temperature in an Engine," *SAE Int. J. Adv. & Curr. Prac. in Mobility* 2, no. 3 (2020): 1303-1313, doi:[10.4271/2020-01-0160](#).
 29. Koutsakis, G., Miles, S., and Ghandhi, J., "Assessment of In-Cylinder Thermal Barrier Coatings over a Full Vehicle Drive Cycle," SAE Technical Paper [2021-01-0456](#) (2021). <https://doi.org/10.4271/2021-01-0456>.
 30. Koutsakis, G., Nellis, G.F., and Ghandhi, J.B., "Surface Temperature of a Multi-Layer Thermal Barrier Coated Wall Subject to an Unsteady Heat Flux," *Int. J. Heat Mass Transfer* 155 (2020), doi:[10.1016/j.ijheatmasstransfer.2020.119645](#).
 31. Koutsakis, G. and Ghandhi, J., "Analytical Solution of Unsteady Heat Conduction in Multilayer Internal Combustion Engine Walls (Under Review)," *Appl. Therm. Eng.* (2022).
 32. Koutsakis, G., Begley, M.R., Hutchinson, J.W., and Ghandhi, J., "Transient Thermo-mechanical Analysis of Reciprocating Engine Thermal Barrier Coatings (Under Review)," *Surf. Coat. Technol.* (2022).
 33. *GT-POWER Engine Performance Application Manual* (Westmont, IL, USA: Gamma Technologies LLC, 2019)
 34. Koutsakis, G., Saputo, J., Gingrich, E., Tess, M. et al., "Delamination Failure on High-Output Diesel Engine Thermal Barrier Coatings," SAE Technical Paper [2022-01-0440](#) (2022). <https://doi.org/10.4271/2022-01-0440>.
 35. Koutsakis, G. and Ghandhi, J., "Optimization of Thermal Barrier Coating Performance and Durability over a Drive Cycle (Under Review)," *Int. J. Eng. Res.* (2022).
 36. Babu, A., Staaden, D., Kokjohn, S., and Dempsey, A., "Emissions Benefits of Group Hole Nozzle Injectors under Conventional Diesel Combustion Conditions," SAE Technical Paper [2020-01-0302](#) (2020). <https://doi.org/10.4271/2020-01-0302>.
 37. Roberts, J., Chuahy, F.D.F., Kokjohn, S.L., and Roy, S., "Isolation of the Parametric Effects of Pre-blended Fuel on Low Load Gasoline Compression Ignition (GCI)," *Fuel* 237 (2019): 522-535, doi:[10.1016/j.fuel.2018.09.150](#).
 38. Roberts, J., Kokjohn, S., Hou, D., and Huang, Y., "Performance of Gasoline Compression Ignition (GCI) with On Demand Reactivity Enhancement," SAE Technical Paper [2018-01-0255](#) (2018). <https://doi.org/10.4271/2018-01-0255>.
 39. Roberts, J.A., "Isolation of Fuel Property and Boundary Condition Effects on Low Load Gasoline Compression Ignition (GCI)," Ph.D Thesis, Mechanical Engineering, University of Wisconsin - Madison, Madison, WI, 2018.
 40. Gatowski, J., Balles, E., Chun, K., Nelson, F. et al., "Heat Release Analysis of Engine Pressure Data," SAE Technical Paper [841359](#) (1984). <https://doi.org/10.4271/841359>.
 41. Dempsey, A.B., "Dual-Fuel Reactivity Controlled Compression Ignition (RCCI) with Alternative Fuels," Ph.D. Thesis, Mechanical Engineering, University of Wisconsin-Madison, Madison, WI, 2013.
 42. ISO 10054:1998 - Internal Combustion Compression-Ignition Engines - Measurement Apparatus for Smoke from Engines Operating Under Steady-State Conditions - Filter-Type Smokemeter, ISO, 1998.
 43. Styron, J., Baldwin, B., Fulton, B., Ives, D. et al., "Ford 2011 6.7L Power Stroke® Diesel Engine Combustion System Development," SAE Technical Paper [2011-01-0415](#) (2011). <https://doi.org/10.4271/2011-01-0415>.
 44. Babu, A. and Kokjohn, S.L., "Cylinder Deactivation Strategies to Stabilize High Stratification Gasoline Compression Ignition Down to Idle," *SAE Int. J. Engines* 14, no. 4 (2021), doi:[10.4271/03-14-04-0035](#).
 45. *Section 610. Duty cycle generation*, "US Code of Federal Regulations - Title 40. Protection of Environment - Chapter I. Environmental Protection Agency - Subchapter U. Air Pollution Controls - Part 1065. Engine Testing Procedures - Subpart G. Calculations and Data Requirements," 2016.
 46. Kajiwara, H., Fujioka, Y., and Negishi, H., "Prediction of Temperatures on Pistons with Cooling Gallery in Diesel Engines using CFD Tool," SAE Technical Paper [2003-01-0986](#) (2003). <https://doi.org/10.4271/2003-01-0986>.
 47. Thiel, N., Weimar, H., Kamp, H., and Windisch, H., "Advanced Piston Cooling Efficiency: A Comparison of Different New Gallery Cooling Concepts," SAE Technical Paper [2007-01-1441](#) (2007). <https://doi.org/10.4271/2007-01-1441>.
 48. Yoshikawa, T. and Reitz, R.D., "Development of an Oil Gallery Cooling Model for Internal Combustion Engines Considering the Cocktail Shaker Effect," *Numer. Heat Transfer, Part A* 56, no. 7 (2009): 563-578, doi:[10.1080/10407780903323512](#).
 49. Vos, K.R., Shaver, G.M., Ramesh, A.K., and McCarthy, J., "Impact of Cylinder Deactivation and Cylinder Cutout via Flexible Valve Actuation on Fuel Efficient Aftertreatment Thermal Management at Curb Idle," *Front. Mech. Eng.* 5 (2019): 52, doi:[10.3389/fmech.2019.00052](#).
 50. Joshi, M.C. et al., "Reducing Diesel Engine Drive Cycle Fuel Consumption through Use of Cylinder Deactivation to Maintain Aftertreatment Component Temperature during Idle and Low Load Operating Conditions," *Front. Mech. Eng.* 3 (2017): 8, doi:[10.3389/fmech.2017.00008](#).
 51. "Direct-injection Engine Research Consortium," <https://derc.wisc.edu/> (accessed 11/24, 2019).